JOURNAL OF GUIDANCE, CONTROL, AND DYNAMICS
Vol. 29, No. 2, March–April 2006

Design and Flight Testing of an $\mathcal{H}_\infty$ Controller for a Robotic Helicopter

M. La Civita*
Carnegie Mellon University, Pittsburgh, Pennsylvania 15213
G. Papageorgiou†
University of Minnesota, Minneapolis, Minnesota 55455
and
W. C. Messner‡ and T. Kanade§
Carnegie Mellon University, Pittsburgh, Pennsylvania 15213

Although robotic helicopters have received increasing interest from university, industry, and military research groups, their flight envelope in autonomous operations remains extremely limited. The absence of high-fidelity simulation models has prevented the use of well-established multivariable control techniques for the design of high-bandwidth control systems. Existing controllers are of low bandwidth and cover only small portions of the vehicle's flight envelope. The results of the synergic use of high-fidelity integrated modeling strategies and robust multivariable control techniques for the rapid and reliable design of a high-bandwidth controller for robotic helicopters are presented. The project implemented and flight tested an $\mathcal{H}_\infty$ loop shaping controller on the Carnegie Mellon University (CMU) Yamaha R-50 robotic helicopter. During the flight tests, the CMU R-50 flew moderate-speed coordinated maneuvers with a level of tracking performance that exceeds performance reported in the publicly available literature. The authors believe that the results open the road to the implementation on robotic helicopters of full-flight-envelope control systems for complex autonomous missions.

Introduction

In recent years, a number of researchers have addressed the design of controllers for robotic helicopters.[1–9] A significant challenge for the control of robotic helicopters is that there is no pilot to compensate for deficiencies in the flight controller, and the reported controllers have achieved quite modest performance: The flight modes are limited to hover and low-speed straight flight, or they lose tracking accuracy considerably as the speed is increased and maneuvering flight is attempted. A large set of design techniques, from classical control to neural-based adaptive control, has been reported. Weilenmann et al.[1] compared, on an indoor bench, several multivariable techniques including $\mathcal{H}_\infty$. The use of $\mathcal{H}_\infty$ control for the design of stability augmentation and guidance systems for fixed- and rotary-wing aircraft has been, by itself, the subject of much research.

Because $\mathcal{H}_\infty$ control can systematically handle uncertain and multi-input/multi-output plants, it promises fast and low-cost design of good-performance flight-control laws. One of the effective $\mathcal{H}_\infty$-based design procedures is called $\mathcal{H}_\infty$ loop shaping[10] and combines the traditional notions of bandwidth and loop gain together with modern ideas of robustness into a single framework. Particular advantages of the method are 1) the ease with which the controller weighting functions can be tuned to give an appropriate system bandwidth and 2) the use of a generalized stability margin that supersedes gain and phase margins. (This is a dimensionless quantity in which a margin of greater than 0.3 is considered good and less than 0.2 unsatisfactory.) Furthermore, controller gain scheduling and antiwindup are easily addressed in the $\mathcal{H}_\infty$ loop-shaping framework because an $\mathcal{H}_\infty$ loop-shaping controller can be written as an exact plant observer plus state feedback.[11]

The approach has now been used quite widely, and a considerable body of experience has been accumulated. To date and to the best of our knowledge, $\mathcal{H}_\infty$ loop shaping is the only type of $\mathcal{H}_\infty$ control that has been flown on a piloted aircraft. A gain scheduled $\mathcal{H}_\infty$ loop-shaping controller flew on the U.K. Defence Evaluation and Research Agency (DERA), now QinetiQ, experimental Harrier aircraft in 1993 (Ref. 12). A fixed-gain two-degree-of-freedom $\mathcal{H}_\infty$ loop shaping controller flew on the National Research Council of Canada's Bell 205 airborne simulator in 1997 (Ref. 13). A self-scheduled linear parameter-varying $\mathcal{H}_\infty$ loop-shaping controller flew on DERA's experimental Harrier aircraft in 1999 (Ref. 14).

In addition to the aforementioned flight tests, a fixed-gain two-degree-of-freedom $\mathcal{H}_\infty$ loop-shaping controller designed for the Westland Lynx multirole combat helicopter[15] and a fixed-gain integrated flight and propulsion $\mathcal{H}_\infty$ loop-shaping controller designed for DERA's experimental Harrier aircraft[16] have been evaluated in piloted simulation. All five control laws were designed in a short amount of time according to AGARD, Gibson, MIL, and ADS-33 specifications and performed satisfactorily, reinforcing our view that $\mathcal{H}_\infty$ loop shaping could indeed benefit the aeronautical industry.

This paper focuses on the design and flight testing of an $\mathcal{H}_\infty$ loop shaping controller for a robotic helicopter. To the best of our knowledge, this paper represents the first complete example of design and test of an $\mathcal{H}_\infty$ loop-shaping controller on any kind of robotic vehicle. A main key to the success of the project has been the integration of $\mathcal{H}_\infty$ loop shaping with a high-fidelity simulation model. This approach has the potential to decrease dramatically the development time of adequate controllers for robotic helicopters. The paper will show that the design complies to several specifications widely used in the rotorcraft community. Finally, the paper will illustrate the flight tests of a set of moderate-speed maneuvers for which the tracking performance exceeds that so far reported in the publicly available literature.

Received 21 June 2002; presented as Paper 2002-4836 at the AIAA Guidance, Navigation, and Control Conference, Monterray, CA, 5–8 August 2002; accepted for publication 1 June 2004.

*Currently Responsible for Technology Innovation, Research and Development Department, Flying-Cam, Rue du Passage d'Eau, 1a, 4681 Oupeye, Belgium; mlacivita@flying-cam.com.

†Senior Scientist, Guidance and Control Section; George.Papageorgiou@honeywell.com.

‡Professor, Department of Mechanical Engineering; bemessner@andrew.cmu.edu.

§Professor, Robotics Institute; tk@cs.cmu.edu.

Robotic Helicopter Model

The Carnegie Mellon University (CMU) Yamaha R-50 (Fig. 1) is a small-scale helicopter designed to be remotely controlled by a human pilot for crop-dusting operations. The R-50 has a two-bladed rotor of 1.535-m radius with a Bell–Hiller stabilizer bar; dry weight is 44 kg, and CMU's instrumentation package adds 23 kg.

The model used is a modeling for flight simulation and control analysis (MOSCA) model.[17] MOSCA is a modeling technique that integrates first-principle and system-identification techniques through the use of global optimization methods in the frequency domain to yield high-fidelity linear and nonlinear models needed for high-bandwidth control design and simulation. The safety pilot flew the helicopter to obtain the frequency sweeps that the computer code CIFER (comprehensive identification from frequency responses) used to generate frequency responses[18] employed by the MOSCA modeling. The controller design employed a linear model extracted at hover, whereas the simulation and evaluation used the nonlinear model before flight testing. The model has 30 states: 9 for the rigid fuselage motion, 6 for the main rotor (tip-path plane representation), 4 for the stabilizer bar, 3 for the Pitt–Peters dynamic inflow model,[19] and 2 for each of the 4 actuators. Keller's wake-distortion parameter[20] is included in the Pitt–Peters dynamic inflow model to correct the typical off-axis mismatch found in many first-principle models. Tail rotor dynamics are represented in a steady-state solution form. Figure 2 shows a comparison at hover for the CMU R-50 between selected flight tests and MOSCA linear model frequency responses.

Fig. 1 CMU robotic helicopter.

Controller Design and Implementation

Background Theory and Design Process

$\mathcal{H}_\infty$ loop shaping, which was proposed by McFarlane and Glover,[10] is a sensible and appealing procedure for designing robust controllers.[21] It is a combination of loop shaping[22] and robust stabilization and is described hereafter.

Step 1

Let $\boldsymbol{G}$ denote a linear time-invariant model of the plant for which the controller is designed. Shape the singular values of $\boldsymbol{G}$ open loop with frequency-dependent weights $\boldsymbol{W}_1$ and $\boldsymbol{W}_2$ according to closed-loop objectives. The weighted plant $\boldsymbol{G}_s = \boldsymbol{W}_2\boldsymbol{G}\boldsymbol{W}_1$ is shown in Fig. 3. What follows is a typical weighting scheme. $\boldsymbol{W}_2$ contains low-pass filters for noise rejection and lead–lag filters for improving robustness. $\boldsymbol{W}_1$ contains proportional and integral filters. The integrators are used to boost the low-frequency gain and, thus, improve output decoupling and tracking and disturbance rejection at both the plant input and output. The proportional matrix gain is used to reduce the

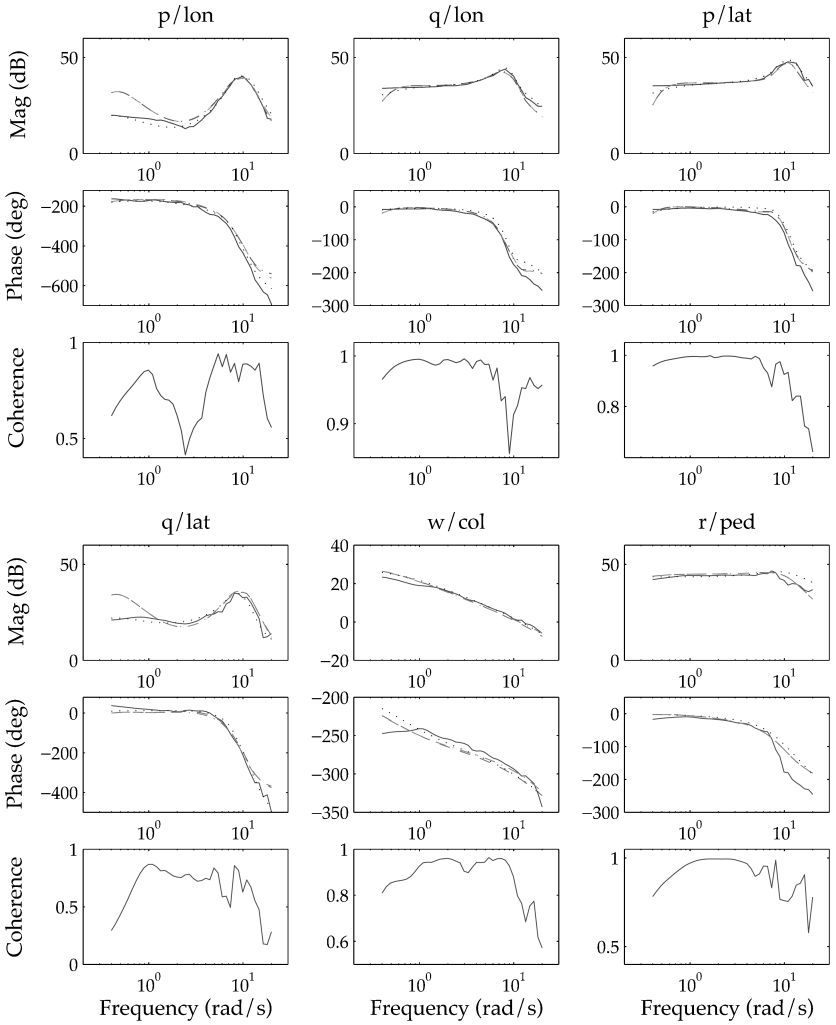

Fig. 2 Hover comparisons: ——, flight tests and – · – · –, MOSCA linear model.

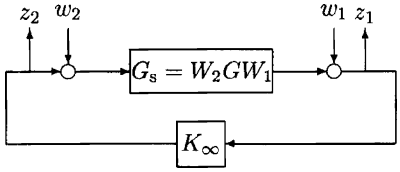

Fig. 3 $\mathcal{H}_\infty$ loop-shaping standard block diagram.

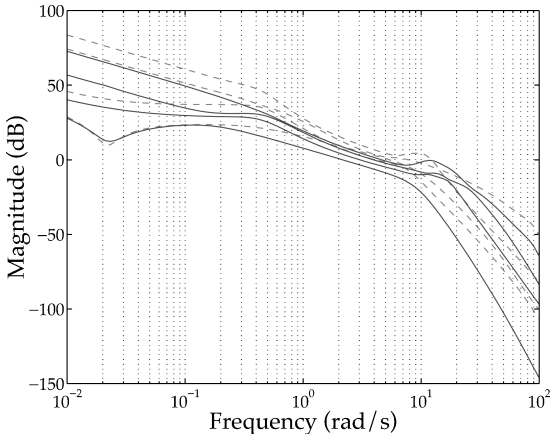

Fig. 4 Singular values of shaped plant with and without $\mathcal{H}_\infty$ controller: – – –, $\sigma(W_2GW_1)$ and ——, $\sigma(W_1K_\infty W_2G)$.

phase lag introduced by the integrators around crossover and to set the actuator usage. The overall gain of $\boldsymbol{W}_1$ and $\boldsymbol{W}_2$ is used to specify the desired loop bandwidth.

Step 2

Maximize the inverse of the $\mathcal{H}_\infty$ norm of the transfer matrix from disturbances $[w_1, w_2]^T$ to errors $[z_1, z_2]^T$ over all stabilizing controllers $\boldsymbol{K}_\infty$, that is,

$$\max_{\text{stab } K_\infty} \left\| \begin{bmatrix} w_1 \\ w_2 \end{bmatrix} \to \begin{bmatrix} z_1 \\ z_2 \end{bmatrix} \right\|_\infty^{-1} = \epsilon$$

The stability margin ϵ takes values in the interval [0, 1] and is a measure of robustness and performance. A margin greater than 0.3 is considered good, based on theory and practical experience. The tradeoff between model accuracy, robustness, performance, and the stability margin ϵ is addressed in Ref. 21.

The theoretical basis for $\mathcal{H}_\infty$ loop shaping is that $\boldsymbol{K}_\infty$ does not modify the desired loop shape $\boldsymbol{G}_s$ significantly at low and high frequencies if the stability margin is not too small.[10] Consider, for example, Fig. 4. The synthesized controller $\boldsymbol{K}_\infty$ achieves an $\epsilon = 0.36$, is essentially a lead–lag filter, and, indeed, does not modify $\boldsymbol{G}_s$ significantly. Therefore, the designer can define performance objectives by shaping the open-loop model $\boldsymbol{G}$ with weights $\boldsymbol{W}_1$ and $\boldsymbol{W}_2$.

Recently, well-established notions of robustness for single-input/single-output systems have been related to the stability margin. It was proved in Ref. 23 that the Nyquist or Nichols plot of any loop transfer function that results from breaking the closed loop at one of the actuators or sensors lies outside a region whose size is a function of the stability margin (Fig. 5). Given the boundary of the region, it is easy to show that the guaranteed single-loop gain margin and phase margin are related to ϵ by

$$\text{GM} = \pm 20 \log_{10}[(1+\epsilon)/(1-\epsilon)], \qquad \text{PM} = 2 \arcsin \epsilon \qquad (1)$$

Thus, a stability margin of 0.35 guarantees gain and phase margins of ±6.3 dB and 40.9 deg, respectively. In Ref. 23 the stability margin is also related to a multi-input/multi-output robustness test popular within the aeronautical industry.

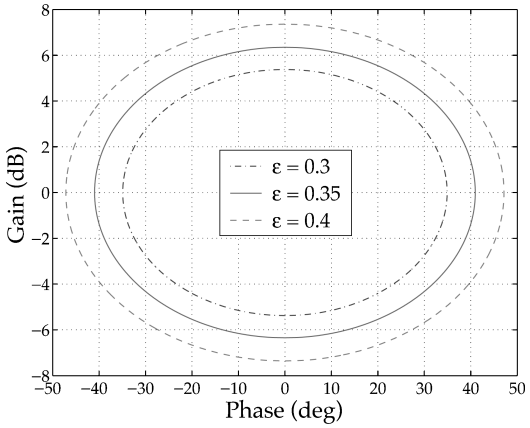

Fig. 5 Guaranteed Nichols plot exclusion regions for $\epsilon = 0.3$, 0.35, and 0.4.

Step 3

Check time simulations and frequency responses of the resulting closed-loop system to verify robust performance. Iterations may be required.

The controller structure implemented on the CMU R-50 is based on an inner-loop and outer-loops architecture: The inner loop (Fig. 6) provides stabilization and decoupling; the outer loops (Figs. 7 and 8) are cascaded with the inner loop for velocity and position control. All loop designs used $\mathcal{H}_\infty$ loop shaping.

Inner-Loop Design and Analysis

The inner loop (Fig. 6) is an attitude-command attitude-hold response type controller. References inputs are pitch attitude θ, roll attitude ϕ, vertical velocity v_z, and yaw rate $\dot{\psi}$. The same four variables were used for feedback. Pitch rate q and roll rate p were not needed in the measurement set because the stabilizer bar already acts as a lagged-rate feedback system.[24]

The oscillatory nature of the angular responses of the R-50 is due to the lightly damped coupling mode between the rotor system and the fuselage evident in the frequency responses of the angular rates to cyclic control inputs (Fig. 2); the stabilizer bar is responsible for the low damping of this mode.[25]

Given the absence of handling qualities requirements for small-scale helicopters, the controller design began by trying to push the bandwidth to be as high as possible while maintaining a good level of robustness. The compilation of a handling qualities standard for robotic helicopters is still an open argument: There are many questions about the kind of missions they will be asked to accomplish, and there is no human pilot onboard requesting and evaluating a set of specific dynamic characteristics. For flight-control problems with mostly qualitative closed-loop specifications, (that is, very few or none of the specifications are quantified, as would probably be the case for an unmanned air vehicle, $\mathcal{H}_\infty$ control can be used to establish the achievable performance quickly. This is because $\mathcal{H}_\infty$ control can systematically handle the multivariable and uncertain nature of the aircraft.

In the $\mathcal{H}_\infty$ loop-shaping framework it is easy to set the system bandwidth, and, thus, the achievable performance would be determined by increasing the system bandwidth until robustness as quantified by the stability multi-input/multi-output margin decreases below the desired level. Furthermore, the use of a high-fidelity model in the controller design provides confidence in the achieved robustness, and it represents accurately the high-bandwidth and multivariable effects that $\mathcal{H}_\infty$ control exploits.

Although a higher level of performance (in particular agility and maneuverability) is generally expected from small-scale helicopters, the CMU R-50 is quite limited in achievable performance. Given the original design aim of the vehicle (crop dusting at limited velocities), together with the relevant payload added by the CMU instrumentation (50% of the machine's dry weight) and the low bandwidth of the actuators (15 rad/s), the use of a set of full-scale helicopters' specifications may be justified. Nevertheless, comparisons with a subset of

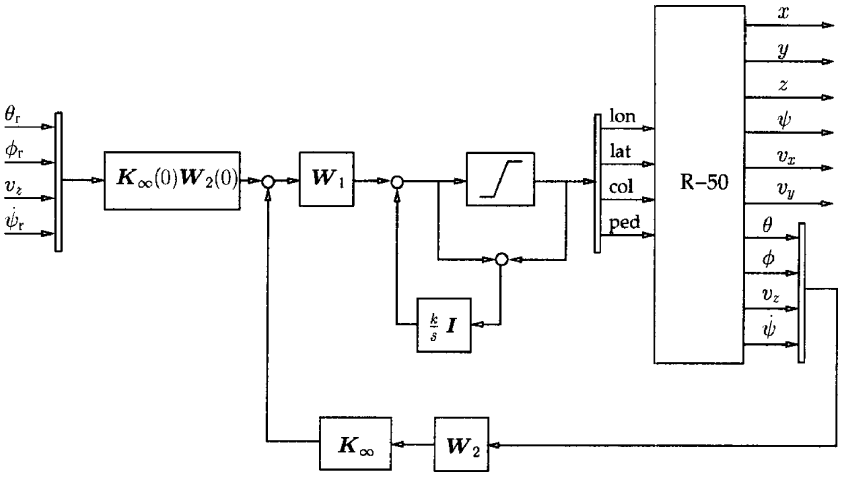

Fig. 6 Inner loop, $K_\infty(0)W_2(0)$ represents the (matrix) dc gains of K_∞ and W_2.

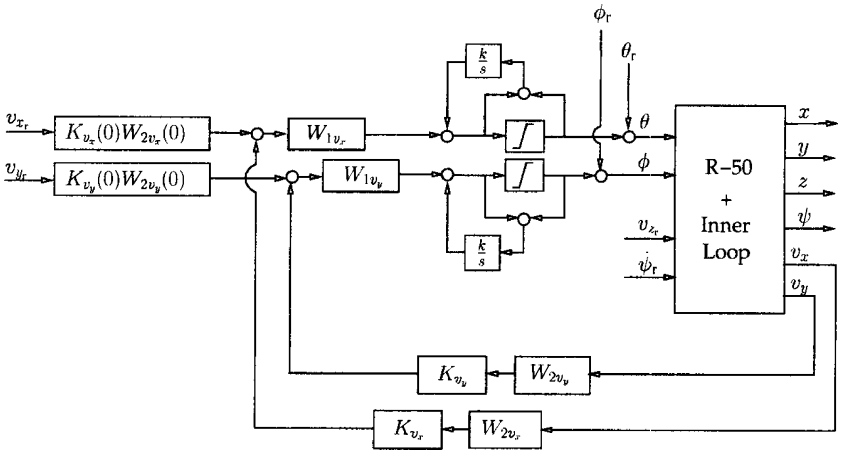

Fig. 7 Outer loops for v_x and v_y control.

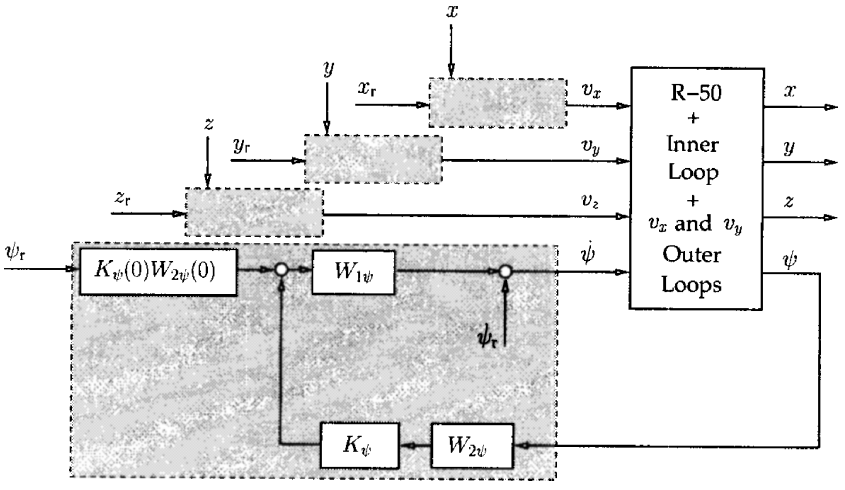

Fig. 8 Outer loops for position control.

the specifications in ADS-33-E (Ref. 26) and MIL-F-9490 (Ref. 27), which contain details about the specifications' metrics, adopted in the full-scale military-helicopter community, showed performance satisfying the requirements with a large margin on the examined bounds.

The requirements for the inner-loop controller are as follows:

1) Stability shall require all of the closed-loop poles to lie in the left half of the s plane.

2) Closed-loop bandwidth ω_{bw} shall satisfy level 1 target acquisition and tracking specifications, which are the highest levels achievable for military rotorcraft in the ADS-33E specifications.

3) In single-loop analysis, gain margin shall be $\geq$6 dB and phase margin $\geq$45 deg to guarantee a reasonable level of robustness.

4) Off-axis responses due to on-axis requests (ϕ/θ_r, θ/ϕ_r, and $\dot{\psi}/v_{z_r}$) shall comply with level 1 aggressive agility specifications.

5) Responses to pulse disturbances injected directly at the inputs of the plant shall return to within 10% of the peak value in 10 s.

These requirements may still be relevant, because there are applications for unmanned helicopters in which a pilot will still perform the guidance and navigation functions, for example, in filmmaking or in some full-scale unmanned helicopters.[28]

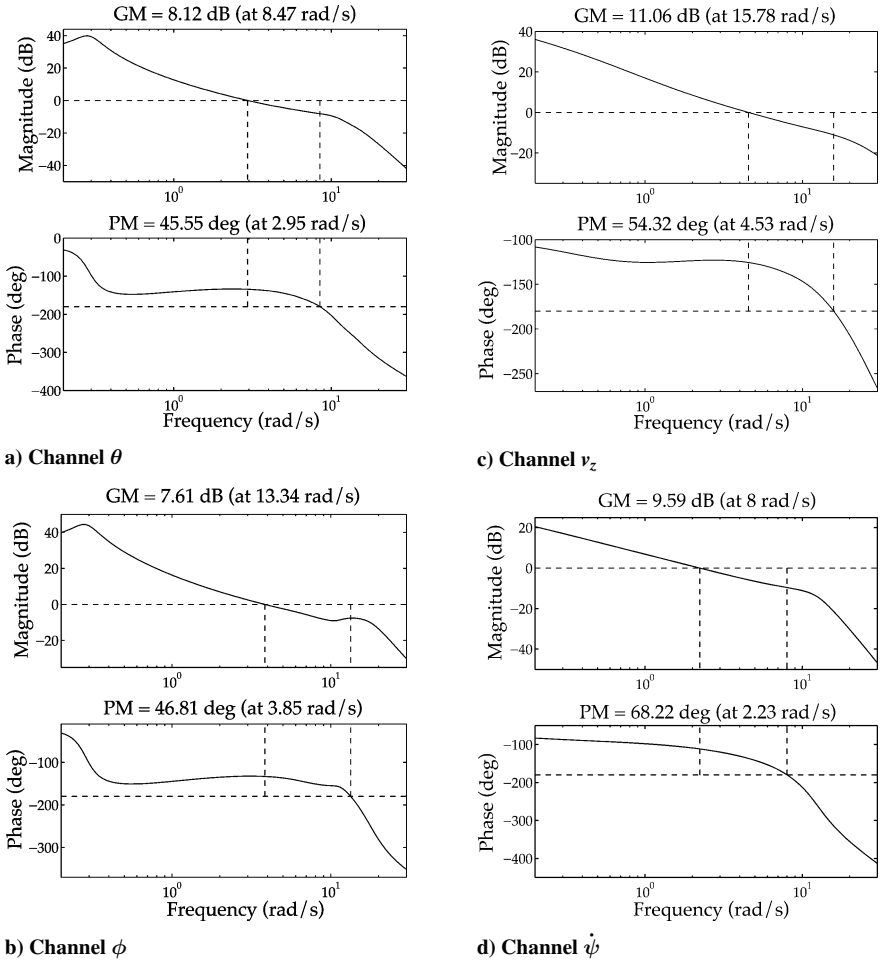

Fig. 9 Bode plots for broken single loop with gain and phase margins.

The design used a diagonal weight $\boldsymbol{W}_1$ with integral action on all the axes; $\boldsymbol{W}_1$ also contains zeros in the θ, ϕ, and v_z axes to decrease rolloff rates at crossover. The complete expression for $\boldsymbol{W}_1$ is

$$\boldsymbol{W}_1 = \text{diag}\left[\frac{1.52s+4.57}{s} \quad \frac{2.23s+6.7}{s} \quad \frac{0.52s+1}{s} \quad \frac{1.45}{s}\right] \tag{2}$$

Diagonal $\boldsymbol{W}_2$, with second-order low-pass filters, provided sensors noise rejection on v_z and $\dot{\psi}$. The complete expression for $\boldsymbol{W}_2$ is

$$\boldsymbol{W}_2 = \text{diag}\left[1.14 \quad 1.0 \quad \frac{2795}{s^2+80s+2500} \quad \frac{2028}{s^2+80s+2500}\right] \tag{3}$$

The diagonal gains of $\boldsymbol{W}_1$ and $\boldsymbol{W}_2$ are tuned to have crossover frequencies of the open-loop system at 7 rad/s. Note that the resulting controller will not be diagonal, even though the weighting matrices are diagonal.

The $\mathcal{H}_\infty$ optimization gave $\epsilon = 0.362$. Figure 4 shows the singular values of the shaped hover model with the $\mathcal{H}_\infty$ controller. The inner-loop controller contains also an antiwindup loop (Fig. 6) based on a classical scheme[29]: A diagonal system with integrators and simple gains feeds back, to the output of $\boldsymbol{W}_1$, the difference between the actual input to the plant and the output from $\boldsymbol{W}_1$. There are two reasons for the presence of an antiwindup loop. First, $\boldsymbol{W}_1$ contains integrators that, in case of actuators' saturation, continue to integrate the error signals causing windup problems (overshoot and rapid degradation of performance). Second, the antiwindup loop ensures a smooth transition (bumpless transfer) between human-pilot mode and computer mode conditioning the $\boldsymbol{W}_1$ while the controller is offline.

Table 1 Bandwidth evaluations with ADS-33E

Channel	ω_{bw}, rad/s	ω_{bw}, ADS-33E, rad/s
θ	5.6	$\geq$2.5
ϕ	9.08	$\geq$2.5
$\dot{\psi}$	6.4	——

Figure 9 shows Bode plots with gain and phase margins for single-loop analysis; all of the loops satisfy the robustness specifications.

The ADS-33E target acquisition and tracking bandwidth requirements for the θ and ϕ channels depend on phase delay, which is less than 0.22 s for the R-50 flight controller. The corresponding bandwidths and specifications are listed in Table 1. In Table 1, ω_{bw} is the frequency where the phase $\Phi = -135$ deg.

The ADS-33E does not specify ω_{bw} for the v_z and $\dot{\psi}$ channels; for the v_z channel, it gives the desired speed of response for the v_z channel in terms of bounds on a time constant $T_{v_z} \leq 5.0$ and a time delay $\tau_{v_z} \leq 0.2$ in a first-order transfer function that matches the step response of the v_z channel. Our controller achieved $T_{v_z} = 0.22$ and $\tau_{v_z} = 0.04$, which satisfy the specified bounds and, thus, enabled the controller to meet all of the inner-loop bandwidth specifications.

ADS-33E describes compliance with level 1 for aggressive agility with bounds on $\Delta\theta_{\text{pk}}/\Delta\phi_4$ and $\Delta\phi_{\text{pk}}/\Delta\theta_4$ for roll and pitch axes: The numerator is the difference between the values (peak within 4 s and at trim) of the off-axis variable caused by a step change of the on-axis variable. The denominator is the difference between the values (at 4 s and at trim) of the on-axis variable. Table 2 lists the calculated values and bounds. Off-axis specification on $v_z/\dot{\psi}$ transfer function

Table 2 Interaxis coupling evaluations with ADS-33E

Evaluation	Value
$\Delta\theta_{pk}/\Delta\phi_4$	0.08
$\Delta\theta_{pk}/\Delta\phi_4$, ADS-33E	$\in \pm 0.25$
$\Delta\phi_{pk}/\Delta\theta_4$	-0.08
$\Delta\phi_{pk}/\Delta\theta_4$, ADS-33E	$\in \pm 0.25$

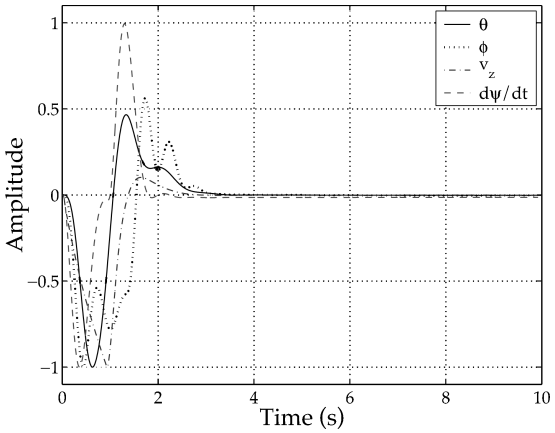

Fig. 10 Nonlinear normalized responses to square pulse disturbances.

requests the presence of a heading (ψ) hold controller. There was no need to test this specification because of the ψ controller on the outer loop.

The last specification is disturbances rejection. Figure 10 shows the nonlinear normalized (with respect to the peak values) responses for each of the four axes when sharp square pulses are applied directly at correspondent plant's input; they all clear the 10% bound well before the 10 s required. The θ and the ϕ responses in Fig. 10 show oscillatory responses that are due to the damping reduction of the coupled rotor/fuselage modes caused by the stabilizer bar. Similar behavior is present in the closed-loop responses to step references. In Ref. 3, the use of notch filters at the input of the plant is proposed to compensate for the effects of the lightly damped modes, that is, to alleviate the reduction in gain margin caused by the resonances, as evident in Fig. 9b, and to avoid exciting the lightly damped modes with fast attitude reference changes.

This choice, besides jeopardizing the robustness of the system with the addition of phase delay at crossover, does not improve the disturbance rejection problem; the effect of disturbances injected at the actuators' input is instead worsened. In fact, the disturbances may still excite the lightly damped mode because they enter the plant without being filtered by the notch filters, and any counteraction of the high-bandwidth feedback controller at the frequency of the underdamped mode is largely reduced by the presence of the notch filters in front of the actuators. If the light oscillatory responses to step reference inputs are of concern, the notch filters may be safely introduced as prefilters at the input of the closed inner loop. A more drastic but better solution would consist of removing the stabilizer bar.[3] However, removing the stabilizer bar would make it very difficult for the safety pilot to fly the helicopter.

Outer-Loops Design and Analysis

The inner-loop closure makes available a high-bandwidth, robust, and decoupled system with four inputs, θ_r, ϕ_r, v_{z_r}, and $\dot{\psi}_r$, and four outputs, θ, ϕ, v_z, and $\dot{\psi}$. The decoupling justifies the use of cascaded single-input/single-output (SISO) outer loops to allow the helicopter to fly a specified trajectory. Before the actual design procedure, balanced model truncation[30] approximated the closed inner loops.

The outer-loops structure uses and controls variables in a special reference frame called the heading referenced inertial coordinate system (HRICS). The HRICS has its origin fixed at the helicopter's c.g., and when $\psi = 0$, the x, y, and z axes are parallel to the Earth frame. If $\theta = a_1, \phi = a_2$, and $\psi = a_3$, the HRICS rotates by a_3 around the z axis of the Earth frame but maintains its z axis parallel to the z axis of the Earth frame, that is, it is unaffected by θ and ϕ angular motions of the helicopter. In the following discussion, the variables for velocities and positions v_x, v_y, v_z, x, y, and z are all assumed to be in the HRICS.

Table 3 Gain and phase margins with broken-loop analysis for velocity outer loops

Loop	Gain margin, dB	Phase margin, deg
v_x	8.23 at 8.39 rad/s	38.07 at 2.74 rad/s
v_y	7.64 at 13.2 rad/s	41.69 at 3.63 rad/s
v_z	11.22 at 16.3 rad/s	55.11 at 4.53 rad/s
$\dot{\psi}$	9.64 at 8.04 rad/s	68.20 at 2.22 rad/s

The first two outer loops (Fig. 7) are closed on the θ and ϕ channels of the inner loop. They allow control of v_x and v_y. For the v_x and v_y channels, ADS-33E contains specifications only for the rise time of their closed-loop response. The other general requirement is the achievement of a good level of robustness measured by gain and phase margin as in MIL-F-9490D.

For both loops, the crossover frequencies were 0.8 rad/s. The $\boldsymbol{W}_1$ weights for each loop have a proportional plus integral structure; the $\boldsymbol{W}_2$ weights contain the same second-order low-pass filters of the inner loop for noise rejection. The $\mathcal{H}_\infty$ optimization gave $\epsilon = 0.374$ for the v_x controller and $\epsilon = 0.398$ for the v_y controller. Notice that these margins refer to the open-loop systems obtained by breaking the v_x and v_y loops at the θ and ϕ reference inputs of the closed inner loop (Fig. 7). Table 3 lists, instead, gain and phase margins obtained by breaking the loops at the plant inputs when the v_x and v_y loops are closed. Note that the phase margins for the loops broken at the longitudinal and lateral cyclic inputs of the plant do not satisfy the requested bounds (phase margin $\geq$45 deg). A possible remedy would be to increase the robustness of the inner-loop design modifying $\boldsymbol{W}_1$ and $\boldsymbol{W}_2$, for example, adding lead–lag filters to decrease the phase delay, or to reduce the bandwidth of the v_x and v_y loops, reducing the gains in the respective $\boldsymbol{W}_1$.

Classical antiwindup loops are also present to prevent windup of the integrators in the $\boldsymbol{W}_1$ weights caused by the limiters on the requested attitude angles. Figures 11a and 11b show step responses for the two loops. The calculated rise times are $T_{v_x} = 2.64$ s and $T_{v_x} = 2.5$ s, which satisfy the specifications in ADS-33E ($2.5 \leq T_v \leq 5.0$). (ADS-33E defines the rise time as the time T necessary to reach 63.2% of the steady-state value.) Figure 11c shows the step response for v_z used in the inner-loop section for T_{v_z} and τ_{v_z} evaluation. This response was obtained with the v_x and v_y loops closed, but simulation indicated that the evaluation of T_{v_z} and τ_{v_z} is practically unchanged when leaving the v_x and v_y loops open.

With the closure of the v_x and v_y outer loops, the main inputs to the systems become v_{x_r}, v_{y_r}, v_{z_r}, and $\dot{\psi}_r$ (Fig. 7); these four channels are utilized by the next four independent SISO outer loops to control x, y, z, and ψ. The controller architecture gives also the possibility to inject θ_r and ϕ_r for feedforward control and turn coordination.

The design of the four position outer loops is analogous to the design of the v_x and v_y loops; x, y, z, and ψ loops are closed, respectively, on v_x, v_y, v_z, and $\dot{\psi}$ (Fig. 8). Again, model reduction on all of the transfer functions for example $x(s)/v_{x_r}(s)$, preceded the closing the four outer loops. The crossover frequencies were 0.6 rad/s for the x and y loops and were 0.8 rad/s for the z and ψ loops. None of the $\boldsymbol{W}_1$ contains integral action because each loop already has a free integrator. (Position is measured in the Earth frame and then transformed in the the heading referenced inertial coordinate system, such that x, y, and z are the integrals of v_x, v_y, and v_z. Yaw angle ψ is by definition the integral of yaw rate $\dot{\psi}$.) To decrease the rolloff rate at crossover, the $\boldsymbol{W}_1$ weights for the x and y loops contain lead–lag filters. The $\boldsymbol{W}_2$ weights are simply unity gains. The $\mathcal{H}_\infty$ optimization gave the following values of ϵ: $\epsilon = 0.59$ for the x loop, $\epsilon = 0.56$ for the y loop, $\epsilon = 0.52$ for the z loop, and $\epsilon = 0.54$ for the ψ loop.

Figures 11d–11f show step responses for the x, y, and ψ loops. For the ψ channel, the ADS-33E requires $\omega_{bw} \geq 3.5$ rad/s. With our

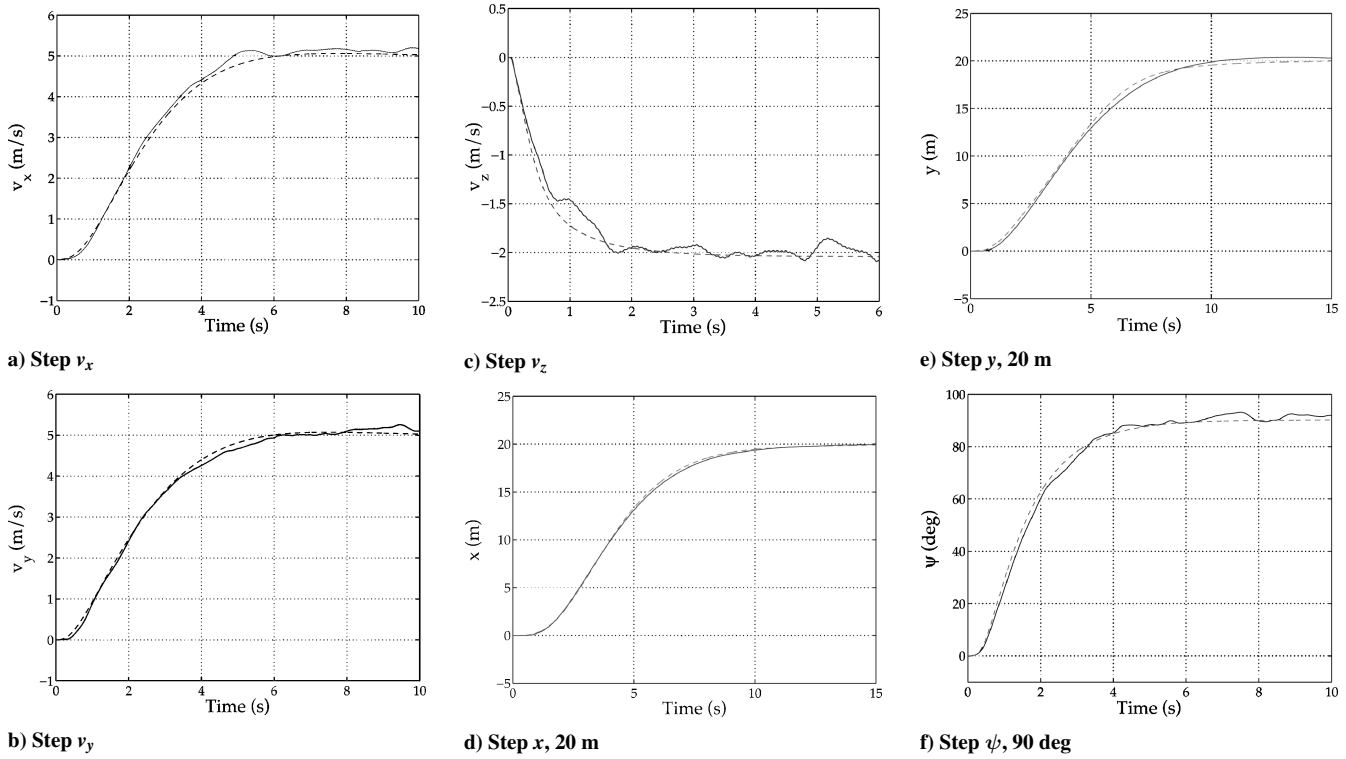

Fig. 11 Step responses v_x, v_y, v_z, x, y, and ψ comparisons between flight tests and MOSCA linear model: ——, flight test and – – –, simulation.

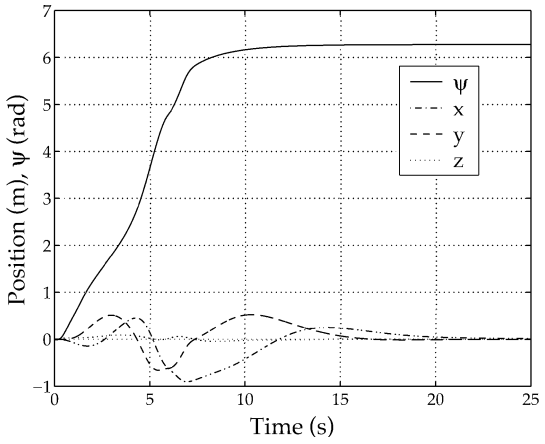

Fig. 12 Turn, 360 deg, with 10-m/s steady wind.

controller structure (ψ controlled in the outer loop) it was impossible to satisfy this specification without a decrease in robustness of the design. The achieved ω_{bw} is 2.5 rad/s. Because the Yamaha R-50 is already equipped with an elementary yaw rate feedback system, a sensible choice would be to eliminate the inner-loop control on $\dot{\psi}$ and control directly ψ instead. This would allow ω_{bw} for ψ to be as high as the one obtained for $\dot{\psi}$ (Table 1) without decreasing the stability margins.

The compliance check for the specifications in ADS-33E for a position-hold controller used the ψ response in Fig. 12. ADS-33E specification for aggressive agility requires that a 360-deg yaw turn be completed in less than 10 s, in steady wind of up to 18 m/s, and maintaining the helicopter position within a 3-m-diam circle at constant altitude. Because the wind during flight tests was not at the level prescribed, a MOSCA nonlinear simulation was necessary. The controller cleared the position and time bounds with a frontal steady wind of 10 m/s. This wind speed is close to an upper limit for the R-50; at larger wind speeds ($\geq$15 m/s), the R-50 lacks tail rotor power to execute the turn, that is, the helicopter stops turning at $\psi = 90$ deg.

The controller architecture leaves the option of directly injecting v_{x_r}, v_{y_r}, v_{z_r}, and $\dot{\psi}_r$ for feedforward control (Fig. 8); it is also possible to switch off any position outer loops in case they are not needed to fly a particular maneuver, for example in straight forward flight the x loop is switched off because the request is on v_x.

Controller Implementation

Controller design and reduction used the MATLAB® μ-Analysis and Synthesis Toolbox.[31] After the reduction, a Tustin bilinear transformation discretized the controller with a 100-Hz sampling frequency. A ground laptop enables updating of gains, weights, filters, and $\mathcal{H}_\infty$ controllers, in flight, without landing the helicopter. After any modification, an ad hoc utility recomputes the new state-space matrices with their dimensions for all of the loops and sends them to the onboard computer through a wireless ethernet connection. Then, the operator or the safety pilot switches in the new controller. More drastic modifications are also possible. In fact, an implemented interface of the high-fidelity nonlinear simulation software MOSCA with MATLAB enabled the following procedure: 1) Modify the helicopter configuration on the field. 2) Update the model. 3) Recompute the controller. 4) Test the controller with nonlinear simulations. 5) Fly test the new system. Possible reconfigurations of the vehicle include, for example, different payloads or weights redistribution.

This aspect is of primary importance because a general criticism of multivariable techniques has always been the difficulty in modifying and tuning the elements of the controller. Once the controller architecture is fixed, $\mathcal{H}_\infty$ loop shaping with automated code generation and high-fidelity simulation models allows the designer to utilize classical loop shaping experience for quick and reliable tuning of the original design. The flight tests tested this procedure. The original outer-loop crossover frequencies were too high and caused undesirable fast attitude changes in the presence of wind gusts. After switching in the baseline controller, the gains of the outer-loops $\boldsymbol{W}_1$s were modified, and a special utility was used to rebuild the whole controller. The new controller was flight tested again without having to land the helicopter.

Flight Tests

The goals of the flight tests were 1) to check the overall performance and robustness of the system and 2) to gain confidence in

flying a set of maneuvers limiting the tracking error within acceptable bounds. The maneuvers were the following:

1) In the forward coordinated turn, the helicopter starts at hover. The operator commands a 6-m/s step in v_x. The helicopter flies on a straight line until the operator commands a turn. All of the loops are engaged except the x position loop because the request is on v_x. The turn trajectory is a circle of 10-m radius R. Once the operator issues the turn command, the helicopter flies the turn while maintaining $v_x = 6$ m/s, $v_y = 0$, constant altitude, and $\dot{\psi} = v_x/R$. The y loop is engaged to drive the horizontal tracking error to zero.

2) The backward coordinated turn is similar to the forward coordinated turn with $v_x = -5$ m/s.

3) In the nose-out pirouette, the helicopter starts at hover. The operator commands a -4-m/s step in v_y. The helicopter flies sideward on a straight line until the operator commands a turn. All of the loops are engaged except the y position loop because the request is on v_y. The turn trajectory is a circle of 10-m radius R. Once the operator issues the turn command, the helicopter flies the turn while maintaining $v_y = -4$ m/s, $v_x = 0$, constant altitude, $\dot{\psi} = v_y/R$, and pointing the tail toward the center of the circle. The x loop is engaged to drive the horizontal tracking error to zero.

4) The nose-in pirouette is similar to the nose-out pirouette with $v_y = 4$ m/s and helicopter's nose toward the center of the circle.

To analyze the data correctly, some comments on the flight tests are needed. The controller was designed for hover operations. Wind gusts of 4–7 m/s were present throughout the tests. Trajectory designs were not intended to be easy to follow, but to test the controller in limiting cases. All of the turn trajectories would require the helicopter to be able to follow, exactly, step changes in attitude and yaw rate to achieve zero tracking error. The operator issued the turn commands following the indications of the safety pilot because these maneuvers were never flown before, and the maximum level of confidence to the safety pilot was essential. The safety pilot relies only on his vision to estimate the flying speed, and it was noticed later that the pilot asked to start all of the turns before the helicopter reached a steady straight flight.

Nevertheless, the tracking performance was quite remarkable, especially considering that, to the best of our knowledge, no other small-scale robotic helicopter has ever flown any coordinated turns at similar speeds. Figure 13 shows the results for the forward coordinated turn. The two dotted vertical lines in Figs. 13c–13f mark the instants when the operator commands straight and turning flight. The horizontal error is less than 2 m, whereas the vertical error is less than 0.3 m. The presence of a constant wind can be clearly seen in Fig. 13c; v_x oscillates with a period equal to the time needed to complete a 360-deg turn. (The completion of the 360-deg turns are marked by the horizontal lines in Fig. 13f. Thus, the constant wind acts as a sinusoidal forcing term.

Figure 14 shows the results for the nose-out pirouette. The two dotted lines have the same meaning as just described. The horizontal error is less than 1 m, and the vertical error is less than 0.2 m.

Videos of the maneuvers in Figs. 13 and 14 and of all of the other described maneuvers can be found online at URL: http://www.roboticflight.org.

Loading Analysis

Some of the robotic helicopter's missions will require extra payload that was not taken into consideration during the controller design. For example, a video camera will be mounted on the helicopter for reconnaissance and filming missions, and some long-distance missions will need extra fuel tanks. This section analyzes the effect of extra payload on the robustness of the inner-loop controller. The robustness of the inner-loop controller will be quantified using single-loop gain and phase margins. The objective of the analysis is to generate loading plots that will enable the helicopter's operator to add extra mass to the helicopter safely.

The first step of the analysis procedure is to generate a linear time-invariant (LTI) model of the helicopter for each loading configuration. Two point masses, m_1 and m_2, were added to the helicopter at coordinates (x, y, z) and $(x, -y, z)$ with respect to the nominal c.g. of the helicopter, where x, y, and z are positive forward, starboard, and downward, respectively. The procedure used the assumptions that $m_1, m_2 \in [0, 5]$ kg, $x \in [-0.2, 0.6]$ m, and $y, z \in [0, 0.4]$ m and that the grid had 6912 configurations. For each loading configuration, it was straightforward to calculate the new mass, c.g., and

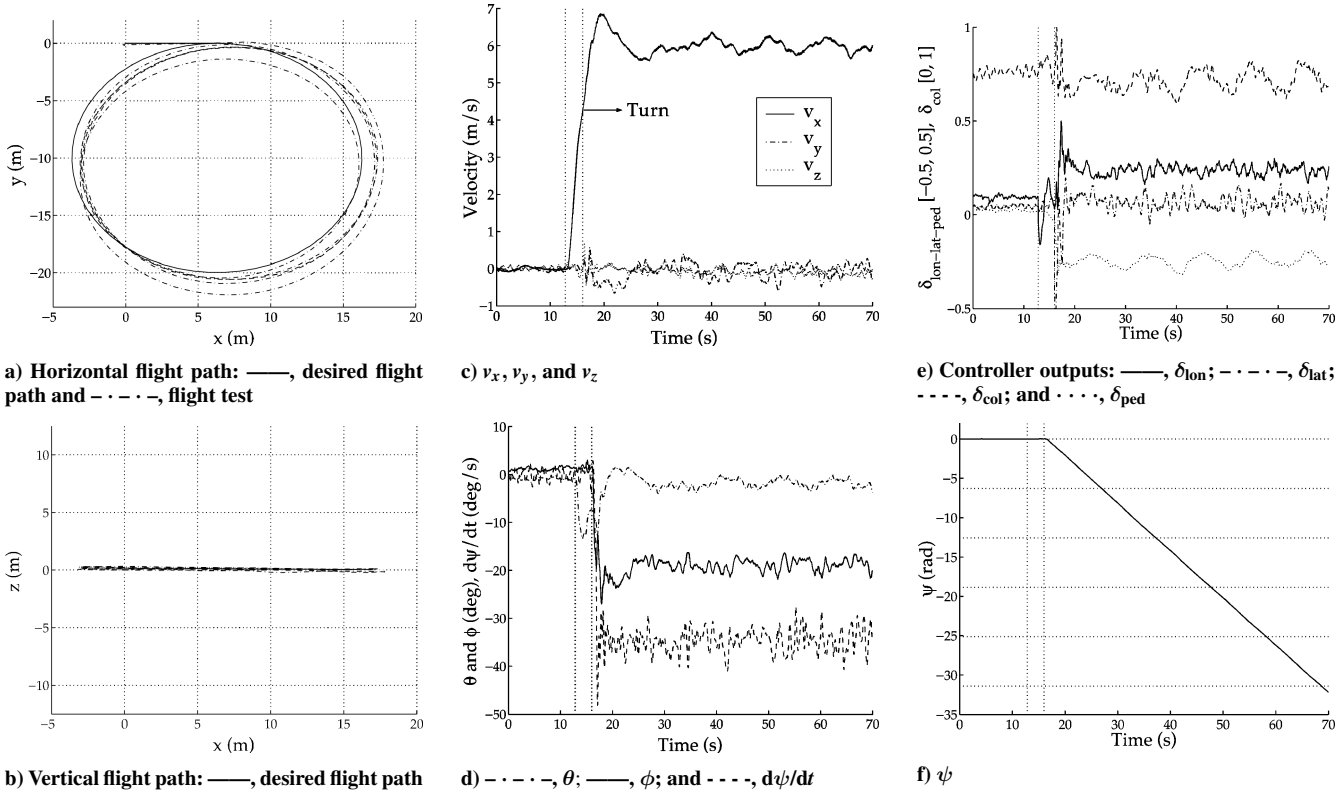

a) Horizontal flight path: ——, desired flight path and – · – · –, flight test

c) v_x, v_y, and v_z

e) Controller outputs: ——, δ_{lon}; – · – · –, δ_{lat}; - - - -, δ_{col}; and · · · ·, δ_{ped}

b) Vertical flight path: ——, desired flight path and – · – · –, flight test

d) – · – · –, θ; ——, ϕ; and - - - -, $d\psi/dt$

f) ψ

Fig. 13 Forward turn, two dotted vertical lines delimit hover, straight, and turn flight.

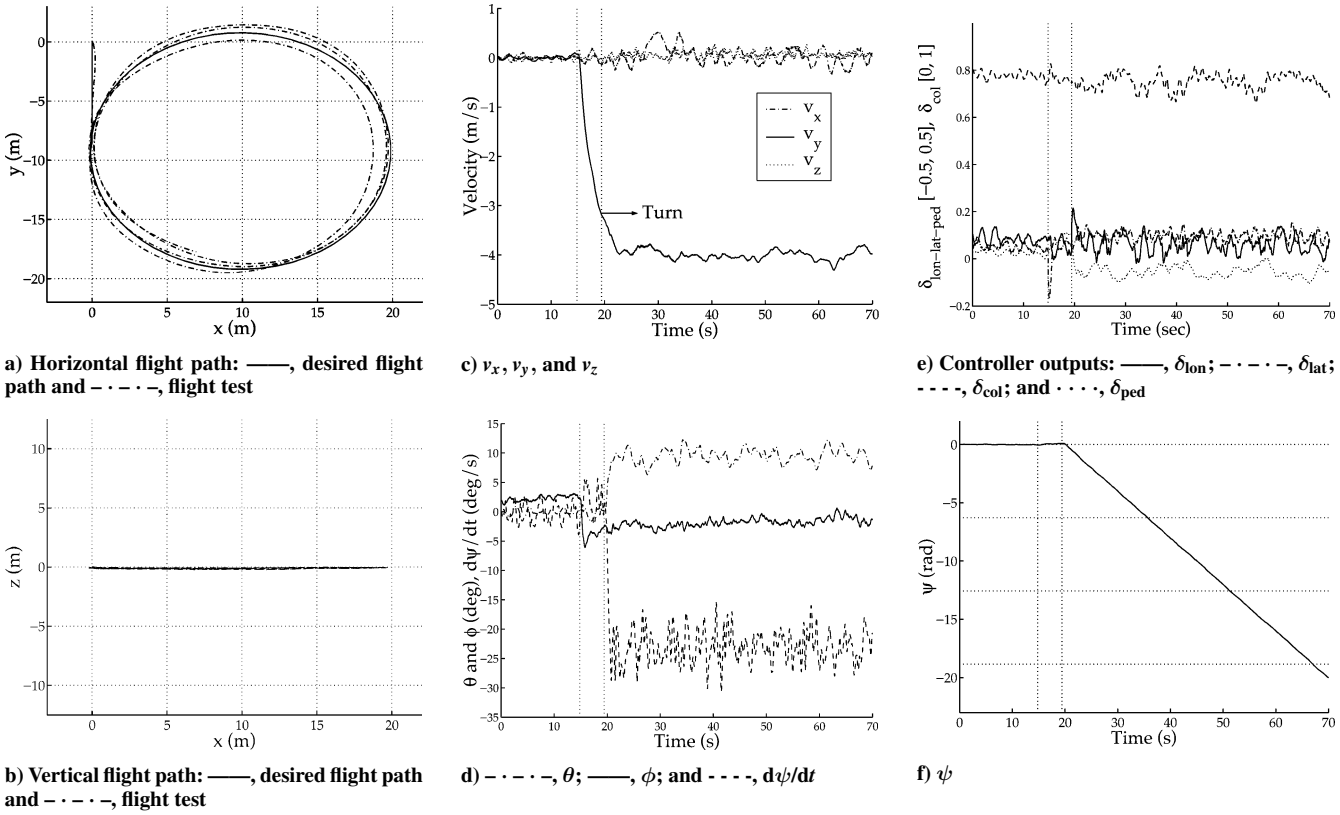

a) Horizontal flight path: ——, desired flight path and – · – · –, flight test

c) v_x, v_y, and v_z

e) Controller outputs: ——, δ_{lon}; – · – · –, δ_{lat}; - - - -, δ_{col}; and · · · ·, δ_{ped}

b) Vertical flight path: ——, desired flight path and – · – · –, flight test

d) – · – · –, θ; ——, ϕ; and - - - -, dψ/dt

f) ψ

Fig. 14 Nose-out pirouette, two dotted vertical lines delimit hover, straight, and turn flight.

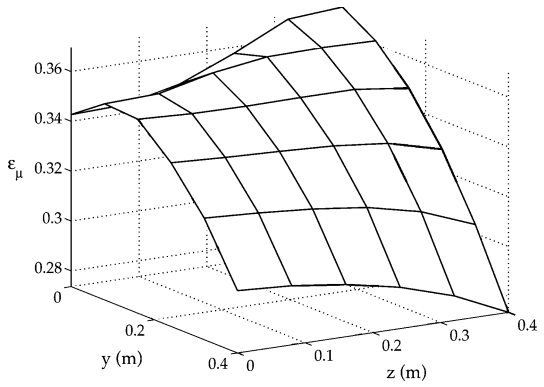

Fig. 15 Loading plot for adding two fuel tanks of different mass (asymmetric loading) at $x = 0.02$ m: ε_μ vs y and z at $x = 0.02$ m with $m_1 = 5$ kg and $m_2 = 1.67$ kg.

moments of inertia of the helicopter and to generate an LTI model using MOSCA.

The second step of the analysis procedure is to compute the single-loop gain and phase margins for each loading configuration. Instead of breaking the closed-loop system at each actuator and sensor and calculating the gain and phase margins of the resulting transfer function, the algorithm computed lower bounds of the worst-case single-loop gain and phase margins. The optimization used to calculate the lower bounds is computationally efficient and does not typically result in conservative lower bounds for robust closed-loop systems.

Let $\boldsymbol{G}_\Delta$ denote the helicopter model at some loading configuration and let $\boldsymbol{K}$ denote the inner-loop controller. The optimization solved is

$$\max_{D} \left\| \boldsymbol{D} \begin{bmatrix} \boldsymbol{I} \\ \boldsymbol{K} \end{bmatrix} (\boldsymbol{I} - \boldsymbol{G}_\Delta \boldsymbol{K})^{-1} [\boldsymbol{I} \quad \boldsymbol{G}_\Delta] \boldsymbol{D}^{-1} \right\|_\infty^{-1} := \epsilon_\mu \qquad (4)$$

The lower bounds of the worst-case single-loop gain and phase margins are obtained by substituting ϵ_μ into Eq. (1). The power of Eq. (4) lies in that ϵ_μ is also related to a multi-input/multi-output robustness test. See Ref. 32 for a more complete explanation of how ϵ_μ is related to single-loop and multiloop gain and phase margins. Note that optimization (4) is straightforward to solve using commercial software, for example, using the μ-tools command mu (Ref. 31).

Figure 15 shows a typical loading plot. It is evident from Fig. 15 that adding two extra fuel tanks of different mass at $x = 0.02$ m anywhere in the y–z plane considered does not decrease ϵ_μ significantly from its nominal value. The worst-case ϵ_μ is 0.274, which corresponds to lower bounds of 4.88 dB and 31.8 deg.

Conclusions

The synergic use of a high-fidelity simulation model and the $\mathcal{H}_\infty$ loop shaping design method proved to be an effective strategy for the rapid and reliable development of a high-bandwidth controller for a robotic helicopter. The design process took only six work months from initial analysis to flight tests. The authors found $\mathcal{H}_\infty$ loop shaping to be more intuitive than other $\mathcal{H}_\infty$ controller design methods. It was possible to explore quickly the design space and understand what level of closed-loop performance was achievable from the system. Classical notions of bandwidth and loop gain allowed choices on performance and robustness tradeoffs.

The synthesized high-bandwidth controller easily satisfied a set of handling-qualities specifications that are a standard in the full-scale military-rotorcraft community. The implementation of the controller on the onboard computer was straightforward. Furthermore, integrating all of the tools used in the design automated the whole process from controller modification to flight test, making it possible to tune the controller in flight. The new controller was capable of flying several moderate-speed coordinated maneuvers that constitute an important step forward in small-scale autonomous helicopter control. The new method also enables analysis of the effect of typical extra-loading conditions on the robustness of the controller. The approach has the potential to lead naturally to the development of a high-bandwidth full-flight-envelope controller for autonomous operations.

Acknowledgments

The authors are grateful to Mark Tischler for supporting part of this project through NASA Grant NAG2-1441. George Papageorgiou was supported by the Defense Advanced Research Projects Agency (DARPA) under the Software Enabled Control (SEC) program, U.S. Air Force Contract F33615-99-C-1497. The DARPA SEC Program Manager is John Bay, with William Koenig and Raymond Bortner (U.S. Air Force Research Laboratory) providing technical support. Dale Van Cleave (U.S. Air Force Research Laboratory) is the Technical Monitor for this contract. The authors thank Omead Amidi, Ryan Miller, and Todd Dudek at CMU for assistance and feedback during flight tests and Noah Falk for designing the graphic interface for MOSCA.

References

[1]Weilenmann, M. F., Christen, U., and Geering, H. P., "Robust Helicopter Position Control at Hover," *American Control Conference*, American Automatic Control Council/Inst. of Electrical and Electronic Engineers, New York, 1994, pp. 2491–2495.

[2]Amidi, O., Kanade, T., and Miller, J. R., "Vision-Based Autonomous Helicopter Research at Carnegie Mellon Robotics Institute 1991–1997," *Heli Japan '98*, American Helicopter Society, Paper T7-3, Alexandria, VA, April 1998.

[3]Mettler, B. F., Tischler, M. B., Kanade, T., and Messner, W. C., "Attitude Control Optimization for a Small-Scale Unmanned Helicopter," AIAA Paper 2000-4059, Aug. 2000.

[4]Koo, T., Shim, D., Shakernia, O., Sinopoli, B., Ma, Y., Ho, F., and Sastry, S., "Hierarchical Hybrid System Design on Berkeley UAV," *International Aerial Robotics Competition*, Association for Unmanned Aerial Vehicle Systems International, Arlington, VA, Aug. 1998.

[5]Hoffman, F., Koo, T., and Shakernia, O., "Evolutionary Design of Helicopter Autopilot," *Advances in Soft Computing: Engineering Design and Manufacturing, (Lecture Notes in Control and Information Sciences)*, edited by R. Roy, T. T. Furuhashi, and P. K. Chawdhry, Springer, London, 1999.

[6]Prasad, J., Calise, A., Pei, Y., and Corban, J. E., "Adaptive Nonlinear Controller Synthesis and Flight Test Evaluation on an Unmanned Helicopter," *Proceedings of the IEEE Conference on Control Applications*, Inst. of Electrical and Electronics Engineers, Piscataway, NJ, 1999, pp. 137–142.

[7]Kim, N., Calise, A. J., Hovakimyan, N., Corban, E., and Prasad, J. V. R., "Adaptive Output Feedback for High-Bandwidth Flight Control," *Journal of Guidance, Control, and Dynamics*, Vol. 25, No. 6, 2002, pp. 993–1002.

[8]Shim, D. H., Kim, H. J., and Sastry, S., "Control System Design for Rotorcraft-Based Unmanned Aerial Vehicles Using Time-Domain System Identification," *IEEE International Conference on Control Applications*, Inst. of Electrical and Electronics Engineers, Paper WM3-5, Piscataway, NJ, 2000, pp. 808–813.

[9]Sprague, K., Gavrilets, V., Dugail, D., Mettler, B., Martinos, I., and Feron, E., "Design and Applications of an Avionics System for a Miniature Acrobatic Helicopter," *20th Digital Avionics Systems Conference*, Vol. 1, Inst. of Electrical and Electronics Engineers, Piscataway, NJ, 2001, pp. 3.C.5-1–3.C.5-10.

[10]McFarlane, D., and Glover, K., "A Loop Shaping Design Procedure Using $\mathcal{H}_\infty$ Synthesis," *IEEE Transactions on Automatic Control*, Vol. 37, No. 6, 1992, pp. 759–769.

[11]Sefton, J. A., and Glover, K., "Pole/Zero Cancellations in the General $\mathcal{H}_\infty$ Problem with Reference to a Two Block Design," *Systems and Control Letters*, Vol. 14, No. 4, 1990, pp. 295–306.

[12]Hyde, R. A., $\mathcal{H}_\infty$ *Aerospace Control Design—A VSTOL Flight Application*, Advances in Industrial Control Series, Springer-Verlag, London, 1995.

[13]Postlethwaite, I., Smerlas, A., Walker, D. J., Gubbels, A. W., Baillie, S. W., Strange, M. E., and Howitt, J., "$\mathcal{H}_\infty$ Control of the NRC Bell 205 Fly-By-Wire Helicopter," *Journal of the American Helicopter Society*, Vol. 44, No. 4, 1999, pp. 276–284.

[14]Papageorgiou, G., and Glover, K., "Taking Robust LPV Control into Flight on the VAAC Harrier," *Proceedings of the 39th IEEE Conference on Decision and Control*, Inst. of Electrical and Electronics Engineers, Piscataway, NJ, 2000, pp. 4558–4564.

[15]Walker, D. J., and Postlethwaite, I., "Advanced Helicopter Flight Control Using Two-Degree-of-Freedom $\mathcal{H}_\infty$ Optimization," *Journal of Guidance, Control, and Dynamics*, Vol. 19, No. 2, 1996, pp. 461–468.

[16]Bates, D. G., Gatley, S. L., Postlethwaite, I., and Berry, A. J., "Design and Piloted Simulation of a Robust Integrated Flight and Propulsion Controller," *Journal of Guidance, Control, and Dynamics*, Vol. 23, No. 2, 2000, pp. 269–277.

[17]La Civita, M., Messner, W. C., and Kanade, T., "Modeling of Small-Scale Helicopters with Integrated First-Principles and System-Identification Techniques," *Proceedings of the 58th Forum of the American Helicopter Society*, Vol. 2, American Helicopter Society, Alexandria, VA, 2002, pp. 2505–2516.

[18]Mettler, B., Tischler, M., and Kanade, T., "System Identification Modeling of a Small-Scale Unmanned Rotorcraft for Flight Control Design," *Journal of the American Helicopter Society*, Vol. 47, No. 1, 2002, pp. 50–63.

[19]Pitt, D. M., and Peters, D. A., "Theoretical Prediction of Dynamic-Inflow Derivatives," *Vertica*, Vol. 5, No. 1, 1981, pp. 21–34.

[20]Keller, J. D., "An Investigation of Helicopter Dynamic Coupling Using an Analytical Model," *Journal of the American Helicopter Society*, Vol. 41, No. 4, 1996, pp. 322–330.

[21]Papageorgiou, G., and Glover, K., "$\mathcal{H}_\infty$ Loop Shaping: Why Is It a Sensible Procedure for Designing Robust Flight Controllers?" AIAA Paper 99-4272, Aug. 1999.

[22]Doyle, J. C., Francis, B. A., and Tannenbaum, A. R., *Feedback Control Theory*, Macmillan, New York, 1992, Chaps. 7, 8, pp. 105–155.

[23]Glover, K., Vinnicombe, G., and Papageorgiou, G., "Guaranteed Multi-Loop Stability Margins and the Gap Metric," *Proceedings of the 39th IEEE Conference on Decision and Control*, Inst. of Electrical and Electronics Engineers, 2000, pp. 4084, 4085.

[24]Miller, R. H., "A Method for Improving the Inherent Stability and Control Characteristics of Helicopters," *Journal of Aeronautical Sciences*, Vol. 17, No. 6, 1950, pp. 363–374.

[25]Heffley, R. K., "A Compilation and Analysis of Helicopter Handling Qualities Data, Volume One: Data Compilation and Volume Two: Data Analysis," NASA CR-3144 and -3145, Aug. 1979.

[26]"Aeronautical Design Standard Performance Specification, Handling Qualities Requirements for Military Rotorcraft," ADS-33E, U.S. Army Aviation and Missile Command, Moffet Field, CA, March 2000.

[27]"General Specification for Flight Control Systems—Design, Installation and Test of Piloted Aircraft," MIL-F-9490D, U.S. Air Force, St. Louis, MO, June 1975.

[28]Frost, C. R., Tischler, M. B., and Bielefield, M., "Design and Test of Flight Control Laws for the Kaman BURRO Unmanned Aerial Vehicle," AIAA Paper 2000-4205, Aug. 2000.

[29]Kothare, M. V., Campo, P. J., Morari, M., and Nett, C. N., "A Unified Framework for the Study of Anti-Windup Designs," *Automatica*, Vol. 30, No. 12, 1994, pp. 1869–1883.

[30]Zhou, K., Doyle, J. C., and Glover, K., *Robust and Optimal Control*, 1st ed., Prentice–Hall, Upper Saddle River, NJ, 1996.

[31]Balas, G. J., Doyle, J. C., Glover, K., Packard, A., and Smith, R., μ*-Analysis and Synthesis Toolbox User's Guide*, 2nd ed., MathWorks, Inc., Natick, MA, 1995.

[32]Papageorgiou, G., and Hyde, R. A., "Analyzing the Stability of NDI-Based Flight Controllers with LPV Methods," AIAA Paper 2001-4039, Aug. 2001.